View metadata, citation and similar papers at core.ac.uk

brought to you by CORE

provided by Elsevier - Publisher Connector

Aerospace Science and Technology 52 (2016) 62–69

Contents lists available at ScienceDirect

Aerospace Science and Technology

www.elsevier.com/locate/aescte

An improved multiple model particle filtering approach for manoeuvring target tracking using airborne GMTI with geographic information

Miao Yu, Hyondong Oh *, Wen-Hua Chen

Department of Aeronautical and Automotive Engineering, Loughborough University, LE11 3TU, UK

ARTICLE INFO

Article history:
Received 16 October 2015
Received in revised form 22 January 2016
Accepted 14 February 2016
Available online 18 February 2016

Keywords:
Manoeuvring ground vehicle tracking
Geographic information
Variable structure multiple models
Particle filter
Particle swarm optimisation

ABSTRACT

This paper proposes a ground vehicle tracking method using an airborne ground moving target indicator radar where the surrounding geographic information is considered to determine vehicle's movement type as well as constrain its positions. Multiple state models corresponding to different movement modes are applied to represent the vehicle's behaviour in different terrain conditions. Based on geographic conditions and multiple state models, a constrained variable structure multiple model particle filter algorithm is proposed. Compared with the traditional multiple model particle filtering schemes, the proposed algorithm utilises a particle swarm optimisation technique which generates more effective particles and generated particles are constrained into the feasible geographic region. Numerical simulation results in a realistic environment show that the proposed method achieves better tracking performance compared with current state-of-the-art ones for manoeuvring vehicle tracking.

© 2016 The Authors. Published by Elsevier Masson SAS. This is an open access article under the CC BY license (http://creativecommons.org/licenses/by/4.0/).

1. Introduction

Airborne surveillance of moving ground targets is one of important capabilities of manned or unmanned aircraft for both military and civil applications such as search and rescue, border patrol, and infrastructure protection, in which the use of airborne ground moving target indicator (GMTI) radar system is of special interest. As mentioned in [1], the GMTI radar system extracts moving ground target information against a stationary background, providing wide-area, all-weather, day/night, and real time capabilities. One important preliminary step for the GMTI based airborne surveillance is to continuously estimate vehicle's state information. For instance, in order to analyse if the behaviour of a vehicle in a surveillance region is normal, its position and velocity need to be extracted [2]. For the continuous estimation of vehicle states, the Kalman or particle filters based on the Bayesian framework are widely applied [3]. Considering a tracked object could manoeuvre with different movement types, the interactive multiple model (IMM) method was applied for state estimation with multiple state models [4]. To overcome the issues of the non-linear measurement model and the non-Gaussian distribution of the noise component, the interactive multiple model particle filter (IMMPF) was proposed in [5], and the simulation results show the improved performance over the standard IMM method.

As the movement of a ground vehicle is not free but constrained by its operational terrain, some terrain information can be combined with certain filtering algorithms. The most widely-used terrain information is the road network, and representative work is shown in [6–9]. In [6], the road constraint was treated as a pseudo-measurement and incorporated into the extended Kalman filter (EKF) scheme for state estimation of the target moving on the road. More advanced algorithms were proposed in [7] using the road map information. The target dynamics was modelled in quasi one-dimensional road coordinates and mapped onto ground coordinates using linear road segments, and Gaussian sum approximations and a particle filtering approach were applied and compared. Cheng et al. in [8] applied a multiple model framework to describe the movement of a vehicle, and the unscented particle filtering scheme was proposed for more effective particle generation. In [9], an interactive multiple model auxiliary particle filtering (IMMAPF) algorithm was applied while considering the road width and multiple state models which describe the different vehicle movements. Arulampalam et al. [10] presented a GMTI vehicle tracking problem in which a vehicle could move on or off road, and a variable structure multiple model (VS-MM) particle filter was applied. The transition probabilities between state models were set in a state dependent way and the active state models were made variable. In [11], instead of using the generic parti-

* Corresponding author.
E-mail address: h.oh@lboro.ac.uk (H. Oh).

http://dx.doi.org/10.1016/j.ast.2016.02.016
1270-9638/© 2016 The Authors. Published by Elsevier Masson SAS. This is an open access article under the CC BY license (http://creativecommons.org/licenses/by/4.0/).

cle filtering approach, the unscented particle filtering scheme was applied in the VS-MM framework to achieve more accurate state estimation with fewer particles.

In this work, a more realistic scenario is considered in which a vehicle manoeuvres in different terrain conditions with different movement types. Note that a vehicle's movement type and position can be determined by different types of terrain. We exploit both the road topology information and the off-road terrain information to aid the GMTI tracking compared with aforementioned works which only take the road topology information into account. In order to deal with the multiple movement types of a manoeuvring vehicle, multiple movement modes are considered and related state models are applied for the vehicle's movement description in a particular terrain, instead of considering only a single movement mode as in [10] and [11]. These geographic information and multiple modes are incorporated into a constrained variable structure multiple model particle filter algorithm, aided by the particle swarm optimisation (denoted as C-VSMM-PSO-PF) for accurate GMTI tracking. The proposed C-VSMM-PSO-PF algorithm applies a particle filtering technique to deal with the non-Gaussian distribution as well as the non-linear GMTI measurements. Different from the algorithms in [10] and [11], a particle swarm optimisation technique ([12] and [13]) is introduced to generate more effective particles within a region with relatively high measurement likelihood values. Particles obtained by performing the PSO which violate the geographic constraints are projected into the feasible geographic regions. The advantages of the proposed C-VSMM-PSO-PF algorithm with Geographic Information System (GIS) information and multiple movement modes are validated via numerical simulations.

This paper is organised as follows. Section 2 presents the geographic information-aided state model and the measurement model for describing the GMTI tracking problem. Section 3 proposes the C-VSMM-PSO-PF algorithm. Section 4 shows the advantages of the proposed ground vehicle tracking method from Monte Carlo simulations in a realistic environment. Conclusions are given in Section 5.

2. GMTI tracking models

This section introduces the state and GMTI measurement models for a GMTI tracking problem. Based on these models, filtering techniques based on the particle filtering framework will be developed for state estimation.

2.1. State model description with geographic information

In a real environment, different types of terrain conditions exist, and the movement of a vehicle is always constrained by terrains whose information can be collected from geographic information systems (GIS) [14]. When a vehicle moves on the road, it moves along the road segment determined by the road topology. For off-road movement, a vehicle moves in a relatively free way but cannot enter inaccessible regions. Thus, different state models are required to describe the state evolution of a vehicle according to the vehicle's movement characteristics in different terrain conditions.

2.1.1. Off-road state model

The state model to describe the off-road movement can be represented as [15]:

$$\mathbf{x}_k^{global} = F\mathbf{x}_{k-1}^{global} + G\mathbf{w}_{global}(m_k) \tag{1}$$

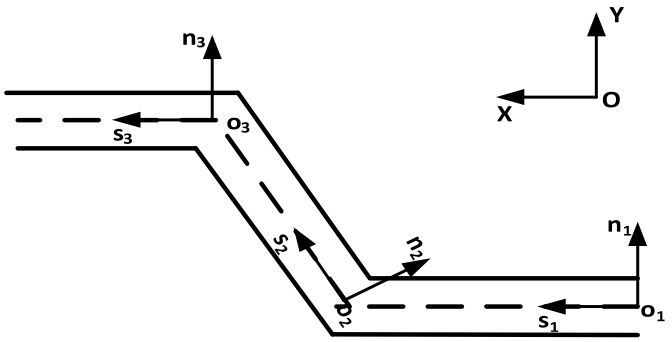

Fig. 1. The representations of local road coordinate systems. $o_1s_1n_1$, $o_2s_2n_2$ and $o_3s_3n_3$ represent local road coordinates with respect to different road segments. *OXY* represents the real world coordinate.

with

$$F = \begin{bmatrix} 1 & 0 & T & 0 \\ 0 & 1 & 0 & T \\ 0 & 0 & 1 & 0 \\ 0 & 0 & 0 & 1 \end{bmatrix}, \quad G = \begin{bmatrix} T^2/2 & 0 \\ 0 & T^2/2 \\ T & 0 \\ 0 & T \end{bmatrix} \tag{2}$$

where $\mathbf{x}_k^{global} = [x_k^{global}, y_k^{global}, \dot{x}_k^{global}, \dot{y}_k^{global}]$ represents the state vector in the real world coordinate system, which includes the real world position ($[x_k^{global}, y_k^{global}]$) and velocity ($[\dot{x}_k^{global}, \dot{y}_k^{global}]$) (here we mainly consider tracking the vehicle's 2-D positions as the height of the vehicle could be derived directly from the GIS as its 2-D positions are known) and T is the interval between consecutive time instances. $\mathbf{w}_{global}(m_k)$ is the uncertain control input of the state model representing the accelerations in different directions. The representation of $\mathbf{w}_{global}(m_k)$ is related to one of the movement modes $m_k \in (CV, CA, Stop)$ considered in this study where $CV, CA, Stop$ represent constant velocity, constant acceleration and stop manoeuvre, respectively.

2.1.2. On-road state model

When a vehicle moves on the road, its movement is determined by the road topology, which mainly follows the road centerline without deviating largely normal to it. In this work, the road network is represented by the connection of straight road segments as in [7] and [8], which represents the road network in a reasonably accurate way while requiring less computational cost. When a vehicle moves on a particular road segment l_k, its corresponding state model is defined as:

$$\mathbf{x}_k^{l_k} = F'\mathbf{x}_{k-1}^{l_k} + G'\mathbf{w}_{l_k}(m_k) \tag{3}$$

with

$$F' = \begin{bmatrix} 1 & T & 0 \\ 0 & 1 & 0 \\ 0 & 0 & 1 \end{bmatrix}, \quad G' = \begin{bmatrix} T^2/2 & 0 \\ T & 0 \\ 0 & T \end{bmatrix} \tag{4}$$

where $\mathbf{x}_k^{l_k} = [s_k^{l_k}, v_k^{l_k}, n_k^{l_k}]$ represents the state associated with the local coordinate system of road segment l_k. As illustrated in Fig. 1, the origin of the local coordinate system is the starting point a road segment (obtained from the GIS) and two axes are along and normal to the road centerline. Inhere, $s_k^{l_k}$ represents the coordinate in the axis along the centerline, $v_k^{l_k}$ is the corresponding velocity and $n_k^{l_k}$ is the coordinate in the axis normal to the centerline. The control parameter $\mathbf{w}_{l_k}(m_k)$ is related both the road segment and one of the on-road movement modes. Similar to the off-road scenario, multiple movement modes are considered to deal with the vehicle manoeuvring with different movement types on the road.

2.1.3. State transition between global/local coordinates

As a vehicle transits from off-road to on-road or vice versa, its state vector representation needs to be transformed between the global real world coordinate system and local road coordinate system for dynamic modelling. For a local state vector $\mathbf{x}_k^{l_t}$, it is converted to its counterpart $\mathbf{x}_t^{global}$ in the real world coordinate system as:

$$x_k^{global} = x_{l_k^{start}} + s_k^{l_k} \cos(\theta_{l_k}) \tag{5}$$

$$y_k^{global} = y_{l_k^{start}} + s_k^{l_k} \sin(\theta_{l_k}) \tag{6}$$

$$\dot{x}_k^{global} = v_k^{l_t} \cos(\theta_{l_k}) \tag{7}$$

$$\dot{y}_k^{global} = v_k^{l_k} \sin(\theta_{l_k}) \tag{8}$$

where $x_{l_k^{start}}$ and $y_{l_k^{start}}$ represent the real world coordinate of the starting point of the current road segment l_k on which a vehicle moves and θ_{l_k} represents the angle of the road segment. $x_{l_k^{start}}$, $y_{l_k^{start}}$ and θ_{l_k} are obtained from GIS. Conversely, $\mathbf{x}_k^{global}$ is converted back to the local state vector $\mathbf{x}_k^{l_k}$ for a particular road segment l_k as:

$$s_k^{l_k} = \sqrt{(x_k^{global} - x_{l_k^{start}})\cos(\theta_{l_k})^2 + (y_k^{global} - y_{l_k^{start}})\sin(\theta_{l_k})^2} \tag{9}$$

$$v_k^{l_k} = \dot{x}_k^{global} \cos(\theta_{l_k}) + \dot{y}_k^{global} \sin(\theta_{l_k}) \tag{10}$$

$$n_k^{l_k} = \frac{|y_k^{global} - x_k^{global} \tan(\theta_{l_k}) + x_{l_k^{start}} \tan(\theta_{l_k}) - y_{l_k^{start}}|}{\sqrt{1 + \tan(\theta_{l_k})^2}}. \tag{11}$$

2.1.4. Terrain type and movement mode transitions

In a real situation, a vehicle might move in different geographic terrains; the movement type of the vehicle also changes due to its manoeuvring. The transition between different terrains is first modelled in a state dependent way by using the distance between the vehicle position and the road entry as:

$$p(r_k = \text{on-road} | r_{k-1} = \text{off-road}) = \exp(-c \cdot d) \tag{12}$$

where d is the distance to the entry point of the road network and c is a positive constant value. The transition probability between the on-road and off-road $p(r_k = \text{off-road} | r_{k-1} = \text{on-road})$ has a similar form as in (12), and the only difference is that the distance d is the one to the exit point of the road. For the movement mode transition, a simple Markov jump model is applied in this work. At time instance $k-1$, we assume that the transition probability to every possible movement modes m_k is equal in order to ensure no bias exists towards a certain movement type.

2.2. GMTI measurement model

A GMTI radar on a UAV platform is assumed to be used, which measures the relative range r and azimuth angle θ of the tracked vehicle, given by:

$$\mathbf{y}_k = \begin{bmatrix} r_k \\ \theta_k \end{bmatrix} = \begin{bmatrix} \sqrt{(x_{o,k} - x_k^{global})^2 + (y_{o,k} - y_k^{global})^2 + (z_{o,k} - z_k^{global})^2} \\ \arctan\left(\frac{y_{o,k} - y_k^{global}}{x_{o,k} - x_k^{global}}\right) \end{bmatrix} + \mathbf{n}_k \tag{13}$$

where $(x_k^{global}, y_k^{global}, z_k^{global})$ and $(x_{o,k}, y_{o,k}, z_{o,k})$ represent the real world position of the tracked vehicle and the observer (GMTI tracker) at time instance k, respectively. $\mathbf{n}_k$ represents the radar measurement noise. There are two issues to be considered for the GMTI radar as described below.

Missed detection A tracked vehicle cannot always be detected. Its detection will be missed if the line-of-sight (LOS) of the GMTI radar to the vehicle is obstructed or the radial velocity (the projected velocity along the line between the GMTI and the tracked vehicle) is below the minimum detection velocity (MDV) (in this case, it is called that the vehicle is within the 'Doppler Blind Zone'). In this work, a similar method to [8] is proposed to model the detection probability considering the effect of the both LOS and MDV as:

$$P_D = \begin{cases} 0, & \text{if a vehicle is outside LOS region or radial velocity is below MDV} \\ p_d, & \text{otherwise} \end{cases} \tag{14}$$

where p_d is a constant between 0 and 1.

False alarms In some cases, false alarms will be generated since anything on the ground with significant motion relative to the sensor can trigger a GMTI detection. These false detections are called 'clutter detections'. It is usually assumed that the number of the clutter detections follows a Poisson distribution and the clutter detections are distributed uniformly across the surveillance region [16].

To deal with the missed detections and false alarms, a general measurement likelihood function is applied to incorporate both the detection probability and clutters distribution, which is represented as [16]:

$$f(\mathbf{Z}_k | \mathbf{x}_k^{global}) \propto 1 - P_D + P_D \sum_{\mathbf{z}_k \in \mathbf{Z}_k} \frac{g(\mathbf{z}_k | \mathbf{x}_k^{global})}{\gamma c(\mathbf{z}_k)} \tag{15}$$

where $\mathbf{Z}_k$ is the measurement set at time instance k which contains both true measurement and false alarms (it could also be an empty set with no measurements), γ the expected number of false alarms per GMTI scan, $c(\mathbf{z}_k)$ the uniform spatial distribution of the false alarm and $g(\mathbf{z}_k | \mathbf{x}_k^{global})$ the likelihood function for a measurement element $\mathbf{z}_k \in \mathbf{Z}_k$ conditioned on the global state $\mathbf{x}_k^{global}$, which is determined according to (13).

3. C-VSMM-PSO-PF algorithm

Considering the following two facts: i) the incorporation of the geographic information into the state equations can significantly distort the distribution of the state vector resulting in a non-Gaussian system and ii) the measurement model of the GMTI radar is non-linear (15), a particle filtering technique is adopted in this work. For the generic particle filtering technique, particles are generated only from predictions by the state models in [10], which introduces outlier particles with low measurement likelihood values. To address this issue, the VSMM-UPF (Unscented Particle Filter) framework [11] was proposed in which unscented Kalman filters were applied for new particles generation. Although this method exploits measurement information for new particles generation, as the unscented Kalman filter is performed for every particle, the algorithm becomes computationally expensive.

To further address the above issue, this paper proposes the constrained variable structure multiple model particle filter algorithm, aided by the particle swarm optimisation (C-VSMM-PSO-PF). Firstly, it uses the particle filtering based on the VSMM framework considering different movement types (on/off movements), different movement modes and state-dependent model transitions between on/off road. The measurement information is incorporated in new particle generation by applying a particle swarm optimisation (PSO) technique to make the outliers move towards

a comparatively high measurement likelihood region. Considering the constraints imposed by the geographic information, the resultant particles are projected into the feasible regions determined by the geographic information. The proposed C-VSMM-PSO-PF algorithm is divided into the following three main steps as follows.

3.1. VSMM prediction

A set of N particles are initialised at $k-1$ as $\{\mathbf{X}_{k-1}^i = [\mathbf{x}_{k-1}^i, l_{k-1}^i, r_{k-1}^i, m_{k-1}^i]\}_{i=1,\ldots,N}$, where each particle $\mathbf{X}_{k-1}^i$ includes the vehicle status (on/off road indicator r_{k-1}^i, movement mode m_{k-1}^i, the particular road segment on which it moves l_{k-1}^i (if r_k^i = off-road, l_{k-1}^i = global)) and the vehicle state vector $\mathbf{x}_{k-1}^i$. New particles for the time instance k are predicted according to the VSMM scheme, which includes:

Status determination. For each particle i, its on/off road indication r_k^i, the road segment l_k^i if it is on-road and the movement mode m_k^i of at time instance k are firstly determined. r_k^i is sampled according to the probability in Eq. (12), m_k^i is chosen from the possible movement modes with an equal probability and l_k^i is determined by the following criteria:

$$l_k^i = \begin{cases} \text{global}, & r_k^i = \text{off-road} \\ l_{start}, & r_{k-1}^i = \text{off-road and } r_k^i = \text{on-road} \\ l_{k-1}^i & r_k^i = \text{on-road} \end{cases} \tag{16}$$

where l_{start} represents the entry to the corresponding road segment.

State prediction. According to $\{l_k^i, r_k^i, m_k^i\}_{i=1,\ldots,N}$ and vehicle states $\{\mathbf{x}_{k-1}^i\}_{i=1,\ldots,N}$ in the particle set, new N vehicle states $\{\mathbf{x}_k^{predict,i,l_k^i}\}_{i=1,\ldots,N}$ are predicted by Eq. (1) (for r_k^i = off-road) or Eq. (2) (for r_k^i = on-road). Note, if $r_k^i \neq r_{k-1}^i$, the corresponding state vector $\mathbf{x}_{k-1}^i$ needs to be transformed accordingly before state prediction.

Status/state adjustment. For r_k^i = on-road and the along-centerline axis coordinate of $\mathbf{x}_k^{predict,i,l_k^i}$ (denoted as s) is larger than the length of the road segment l_k^i (denoted as L) or smaller than zero, a new road segment which connects to the end or start point of the road segment l_k^i is chosen to replace the original l_k^i. The coordinate in the along-centerline axis of $\mathbf{x}_k^{predict,i,l_k^i}$ is adjusted to $s_k^{predict,i,l_k^i} - L$ or $-s_k^{predict,i,l_k^i}$. After the VSMM prediction step, a new set of particles $\{\mathbf{X}_k^{predict,i} = [\mathbf{x}_k^{predict,i,l_k^i}, l_k^i, r_k^i, m_k^i]\}_{i=1,\ldots,N}$ is obtained.

3.2. Particle swarm optimisation

Note that a set of particles $\{\mathbf{x}_k^{predict,i,l_k^i}\}_{i=1,\ldots,N}$ may fall into a very low measurement likelihood region. To mitigate this issue, the particle swarm optimisation (PSO) [12], a population based stochastic optimisation technique, is applied to make the predicted vehicle states move into a comparatively high measurement likelihood region (as illustrated in Fig. 2) by maximising the likelihood function in Eq. (15).

The predicted states $\{\mathbf{x}_k^{predict,i,l_k^i}\}_{i=1,\ldots,N}$ are taken as an initial population set for the PSO algorithm. For the consensus of the vehicle states' coordinates, all the vehicle states are transformed into the real word coordinate system as $\{\mathbf{x}_k^{predict,i,global}\}_{i=1,\ldots,N}$ using Eqs. (5)–(6). Then, for each $\mathbf{x}_k^{predict,i,global}$, a fitness value

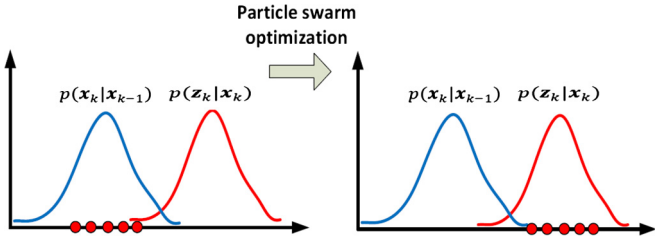

Fig. 2. The illustration of particle swarm optimisation, which makes particles generated from the state transition probability converge into a region with comparatively high measurement likelihood value.

$f(\mathbf{Z}_k|\mathbf{x}_k^{predict,i,global})$ is calculated. Based on individual best position $\mathbf{p}_0^i$ and global best $\mathbf{g}_0$, every individual i moves with a velocity of $\mathbf{v}_0^i$, which relates to the difference between the individual i and the individual and global best, which constructs a new population set. Using this new population set, the same procedure repeats to obtain individuals with higher fitness values. The population set update continues until certain conditions are met (e.g. the maximum iteration number is reached or the function values for the majority of points are larger than a pre-specified threshold, as will be illustrated in the numerical simulations section).

Technical details of the PSO are explained in Algorithm 1. r_1 and r_2 in Algorithm 1 are random numbers with Gaussian distribution $N(0,1)$, and ρ is a zero-mean Gaussian perturbation noise added to avoid particles being trapped in local optima. The obtained population set after performing the PSO, $\{\mathbf{X}_k^{optimised,i} = [\mathbf{x}_k^{optimised,i}, l_k^i, r_k^i, m_k^i]\}_{i=1,\ldots,N}$ is obtained to replace the original set $\{\mathbf{x}_k^{predict,i,l_k^i}\}_{i=1,\ldots,N}$ for a new set of particles.

Algorithm 1 Particle swarm optimisation to obtain more effective particles.

Input: $\{\mathbf{x}_0^i\}_{i=1,\ldots,N} = \{\mathbf{x}_k^{predict,i,global}\}_{i=1,\ldots,N}$ is chosen as the initial population set.
1: Set $j=0$, $\mathbf{p}_0^i = \mathbf{x}_0^i$ for $i=1,\ldots,N$, $\mathbf{g}_0 = \arg\max_{\mathbf{p}_0^i} f(\mathbf{Z}_k|\mathbf{p}_0^i)$ for $i=1,\ldots,N$
2: **while** Termination condition is not met **do**
3: $j = j+1$
4: **for** i = 1 to N **do**
5: $\mathbf{v}_j^i = |r_1|(\mathbf{p}_{j-1}^i - \mathbf{x}_{j-1}^i) + |r_2|(\mathbf{g}_{j-1} - \mathbf{x}_{j-1}^i) + \rho$
6: $\mathbf{x}_j^i = \mathbf{x}_{j-1}^i + \mathbf{v}_j^i$
7: $\mathbf{p}_j^i = \begin{cases} \mathbf{x}_j^i & \text{if } f(\mathbf{Z}_k|\mathbf{x}_j^i) > f(\mathbf{Z}_k|\mathbf{p}_{j-1}^i), \\ \mathbf{p}_{j-1}^i & \text{otherwise.} \end{cases}$
8: **end for**
9: $\mathbf{g}_j = \arg\max_{\mathbf{p}_j^i} f(\mathbf{Z}_k|\mathbf{p}_j^i)$ for $i=1,\ldots,N$
10: **end while**
Output: $\{\mathbf{x}_k^{optimised}\}_{i=1,\ldots,N} = \mathbf{g}_j$

3.3. Particles projection and state estimation

Finally, the geographic information which constrains the vehicle's movement is considered. As the geographic constraint regions are often non-linear, a projection based method [17] which is a simple but efficient technique to deal with different types of constraints, is applied to exploit the geographic constraint information. For the particle $\mathbf{X}_k^{optimised,i} = [\mathbf{x}_k^{optimised,i}, l_k^i, r_k^i, m_k^i]$ obtained from the PSO process, if the vehicle position is not within the feasible region (outside the road boundary if r_k^i = on-road or inside the off-road infeasible region if r_k^i = off-road), then it is projected to the nearest point on the feasible region boundary. The particles after projection are denoted as $\{\mathbf{X}_k^{projection,i} = [\mathbf{x}_k^{projection,i}, l_k^i, r_k^i, m_k^i]\}_{i=1,\ldots,N}$.

The probability of a vehicle being on/off road $p(r_k)$, the movement mode probability $p(m_k)$ and the state estimation $\hat{\mathbf{x}}_k^{m,r}$ corre-

sponding to an off/on road movement type ($r_k = r$) with a particular movement mode ($m_k = m$) are obtained as:

$$p(r_k = r) = \sum_i w_i, \quad \text{for } i \in \{j | r_k^j = r\} \tag{17}$$

$$p(m_k = m) = \sum_i w_i, \quad \text{for } i \in \{j | m_k^j = m\} \tag{18}$$

$$\hat{\mathbf{x}}_k^{m,r} = \frac{\sum_i w_i \mathbf{x}_k^{projection,i}}{p(m_k = m, r_k = r)}, \quad \text{for } i \in \{j | r_k^j = r, m_k^j = m\} \tag{19}$$

where $w_i \propto f(\mathbf{Z}_k | \mathbf{x}_k^{projection,i})$ as in Eq. (15).

The on/off road type (denoted as $r_{vehicle}$) and the movement mode (denoted as $m_{vehicle}$) of the vehicle are determined from the largest $p(r_k)$ and $p(m_k)$. The final state estimation of the vehicle is then $\hat{\mathbf{x}}_k^{m_{vehicle}, r_{vehicle}}$. After the state estimation, for every particle i whose $r_k^i =$ on-road, the vehicle state vector $\mathbf{x}_k^{projection,i}$ is converted back to the local coordinate for the VSMM prediction at the next time instance using Eq. (9). The outline of the proposed C-VSMM-PSO-PF algorithm is presented in Algorithm 2:

Algorithm 2 The outline of the C-VSMM-PSO-PF algorithm.

Input: N particles are initialised at $k-1$ as $\{\mathbf{X}_{k-1}^i = [\mathbf{x}_{k-1}^{i,l_{k-1}^i}, l_{k-1}^i, r_{k-1}^i, m_{k-1}^i]\}_{i=1,\ldots,N}$

- *VSMM prediction:*
  Obtaining the on/off road movement type r_k^i, road segment l_k^i movement mode m_k^i and predicted state $\mathbf{x}_k^{i,l_k^i}$ according to corresponding transition probabilities for every particle. Every predicted state $\mathbf{x}_k^{predict,i,l_k^i}$ is converted to the global one $\mathbf{x}_k^{predict,i,global}$ for PSO.
- *PSO:*
  Taking the predicted vehicle states $\{[\mathbf{x}_k^{predict,i,global}\}_{i=1,\ldots,N}$ as an initial population, a new set of vehicle states $\{\mathbf{x}_k^{optimised,i}\}_{i=1,\ldots,N}$ is obtained from PSO using Algorithm 1
- *Particle projection:*
  For the obtained vehicle state particles $\mathbf{x}_k^{\text{optimised},i}$ whose position is outside the feasible region, we project the vehicle position to the nearest point on the feasible region's boundary to obtain a new set of vehicle state particles $\{\mathbf{x}_k^{projection,i}\}_{i=1,\ldots,N}$.
- *State estimation:*
  The final particle set at time instance k is obtained as $\{\mathbf{X}_k^i = [\mathbf{x}_k^{projection,i}, l_k^i, r_k^i, m_k^i]\}_{i=1,\ldots,N}$. The on/off road probability, movement mode probability and vehicle state are obtained using Eqs. (17)–(19). After the state estimation, the corresponding $\mathbf{x}_k^{projection,i}$ is converted back to the local road segment state for $r_k^i =$ on-road. The VSMM prediction for the next time instance is then performed and the above procedure repeats.

4. Numerical simulations

The advantages of the proposed C-VSMM-PSO-PF algorithm are evaluated by numerical simulations. We simulate a scenario that an unmanned aerial vehicle (UAV) with the GMTI radar tracks a highly manoeuvring vehicle in a realistic environment (a region of Lindifferon, St. Andrews in the United Kingdom). The simulated vehicle trajectory is plotted as the blue line in Fig. 3. x and y axes represent the distance to the origin along the East and North direction, respectively.

The on/off road transition, movement modes transitions and velocity amplitude variations corresponding to the simulated vehicle movement are plotted in Fig. 4. The state models corresponding to on/off road movements have forms of Eqs. (1) and (3) as described in Section 2, and three types of movement modes (CV, CA and Stop) are considered in this work. The control parameter $\mathbf{w}_{global}(m_k)$ for the off-road movement with different movement modes is set as:

Fig. 3. The trajectories of the simulated UAV (red stars) and vehicle (blue line) movements. The satellite image is taken from Google Earth and geo-referenced. (For interpretation of the references to colour in this figure legend, the reader is referred to the web version of this article.)

$$\mathbf{w}_{global}(m_k) \sim N(\mathbf{w}|\mathbf{0}, \begin{bmatrix} (0.1)^2 & 0 \\ 0 & (0.1)^2 \end{bmatrix}) \text{ for } (m_k = CV)$$

$$\mathbf{w}_{global}(m_k) \sim N(\mathbf{w}|\mathbf{0}, \begin{bmatrix} (15)^2 & 0 \\ 0 & (15)^2 \end{bmatrix}) \text{ for } (m_k = CA)$$

$$\mathbf{w}_{global}(m_k) = \begin{bmatrix} -\dot{x}_k^{global} \\ -\dot{y}_k^{global} \end{bmatrix} \text{ for } (m_k = Stop) \tag{20}$$

where $\mathbf{w}_{global}(m_k)$ is assumed to follow Gaussian distribution for CV and CA movement mode. The standard deviations of the components of $\mathbf{w}_{global}(m_k)$ are set to be small for CV to reflect the movement with a constant velocity and those for the CA mode are set large to deal with the vehicle manoeuvring. Similarly, the control parameter $\mathbf{w}_{onroad}(m_k)$ of the on-road state model corresponding to different on-road vehicle in Eq. (21) is set as:

$$\mathbf{w}_{l_k}(m_k) \sim N(\mathbf{w}|\mathbf{0}, \begin{bmatrix} (0.1)^2 & 0 \\ 0 & \sigma_n^2(l_k) \end{bmatrix}) \text{ for } (m_k = CV)$$

$$\mathbf{w}_{l_k}(m_k) \sim N(\mathbf{w}|\mathbf{0}, \begin{bmatrix} (15)^2 & 0 \\ 0 & \sigma_n^2(l_k) \end{bmatrix}) \text{ for } (m_k = CA)$$

$$\mathbf{w}_{l_k}(m_k) = \begin{bmatrix} -v_k^{l_k} \\ 0 \end{bmatrix} \text{ for } (m_k = Stop) \tag{21}$$

where the standard deviation for the first component of $\mathbf{w}_{l_k}(m_k)$ (representing the acceleration along the road centerline) is set in the same way as in the off-road movement scenario. The second component of $\mathbf{w}_{l_k}(m_k)$ represents the change of the normal distance for consecutive time instances whose standard deviation $\sigma_n(l_k)$ is related to the width of the particular road segment l_k (obtained from the GIS).

A GMTI radar sensor is assumed to be mounted on a moving UAV platform for ground surveillance. We simulate the UAV loitering at an altitude of 200 m where the circle radius is 100 m and angular speed is $\pi/20$ rad/s (the UAV trajectory in the 2-D overlook plane is marked as red stars in Fig. 3). Measurements of the GMTI radar are simulated according to Eq. (13) with a Gaussian noise being added to the relative range and angle between the vehicle and the UAV platform. The Gaussian noise is assumed to have zero mean and the standard deviations for r and θ are: $\sigma_r = 5$ m and $\sigma_\theta = 0.05$ rad, respectively. It is assumed that the vehicle is always within the line-of-sight of the sensor. If the radial velocity between the vehicle and the GMTI radar is smaller than the threshold (set to 1 m/s in this work), no vehicle measurements are obtained; otherwise, corresponding measurements are generated with a detection probability of p_d which is set to be 0.9. The expected number of false alarms (γ in Eq. (15)) is set to 2 and false alarms are assumed to be spatially equally distributed across the surveillance area in Fig. 3.

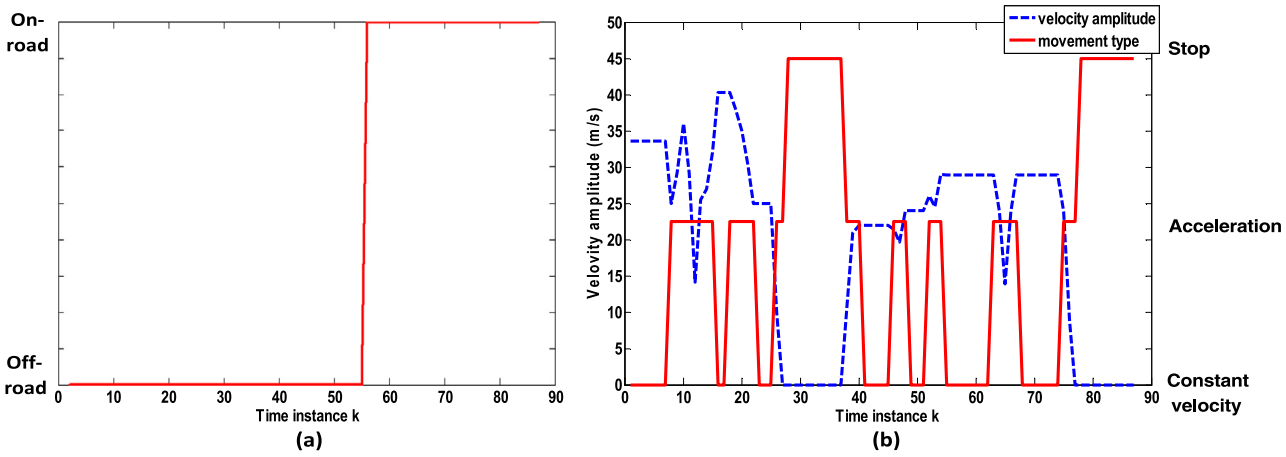

Fig. 4. The transitions of the vehicle's movement types. (a) on/off road movement transitions (b) velocity and movement mode variations.

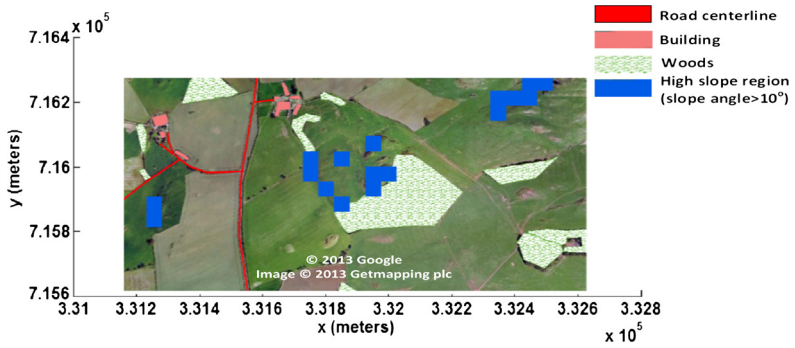

Fig. 5. The presentation of different types of terrains on a georeferenced image. Terrain information is obtained from GIS.

The geographic information for the surveillance area is obtained from the GIS. In the GIS, different types of terrains such as the off-road wood/building regions or the road network and their corresponding geographic information (area of a terrain region, real world positions, region boundary, etc.) are available from corresponding geographic datasets. Fig. 5 represents the visualisation of different types of terrain regions on a geo-referenced image in the surveillance area, obtained from the Ordnance Survey OpenData [18]. Based on this simulation scenario, evaluations are performed as described below.

4.1. PSO termination conditions

The termination conditions of the PSO in our proposed C-VSMM-PSO-PF algorithm are set as: i) values of measurement likelihood function (15) for a certain amount of particles (50% of the entire particle number in the algorithm implementation) are not smaller than a particular threshold (set by 0.1); or ii) the maximum allowed iteration number (denoted as i_{max}) is reached. Condition i) guarantees that a certain percentage of particles are not 'outliers' but in a comparatively high measurement likelihood region with proper levels of likelihood function values and condition. Condition ii) determines the maximum allowed execution time of the PSO algorithm.

We evaluate the influences of different i_{max} on the performance of our algorithm. The comparison results are shown in Table 1, from which we can see that as i_{max} increases, smaller mean and standard deviation of RMSE errors are obtained. However, as i_{max} reaches to a certain value, the additional increase of i_{max} will not result in much improvements. For example, as the i_{max} increases from 5 to 10, there is a reduction of 3.46 (corresponding to 24% reduction) of the RMSEs mean. However, as the i_{max} increases from 10 to 20, the reduction of the RMSEs mean is only 0.12 (corresponding to 1% reduction). Thus, $i_{max} = 10$ is chosen for the evaluations in the following sections.

Table 1
The performance comparison for different maximum PSO iterations.

i_{max} value	Mean (m)	Std (m)	Computation time (s)
0	19.14	2.90	3.18
5	14.53	2.05	3.66
10	11.07	1.15	4.30
20	10.95	1.07	4.49

4.2. Geographic information evaluation

Next, we analyse the effect of incorporating the geographic information in terms of the tracking performance. The proposed algorithm is compared with its counterpart without incorporating any GIS information. If no geographical information is used, the state model in Eq. (1) is always applied to describe the vehicle movement. Otherwise, different models mentioned in Section 2 are applied to describe the on/off road movements and the infeasible region (including the woods, building and high slope regions as marked in Fig. 5 and regions outside the road boundary when the vehicle moves on road) are exploited to constrain the particles.

50 trials of Monte-Carlo simulations are performed (and this applies to the rest of this section). At every time instance, the averaged root mean square errors (RMSEs) between tracking results and ground truth trajectory are plotted in Fig. 6(a) and averaged on/off road probabilities are plotted in Fig. 6(b). The error mean and standard deviation are presented in Table 2. From the results, we can see that estimated on/off road probabilities

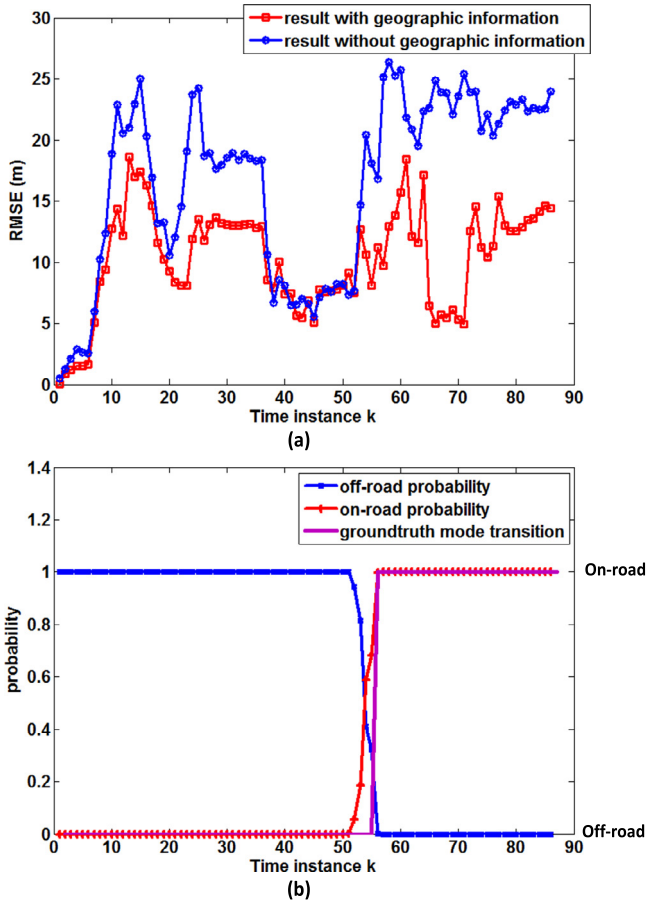

Fig. 6. The 50 times averaged RMSEs and on/off road probabilities for every time instance. (a) The comparison of 50 times averaged RMSEs at every time instances for approaches with/without geographic information. (b) The 50 times averaged on/off road probabilities.

Table 2
The estimation performance comparison with and without the geographic information.

	Mean (m)	Std (m)
No geographic information	19.42	2.43
Geographic information	11.07	1.15

are closely matched with the ground truth and by incorporating the geographic information, improved tracking performance is obtained with more than 40% improvement of the mean tracking error.

4.3. Evaluation of incorporating multiple movement modes

We also analyse the advantage of considering three different movement modes ($m_t = CV$, CA and *Stop*) for describing both the on and off road movements. We compare our multiple movement mode scheme with the one in [10] and [11] which only considers a single movement mode. For the single movement mode scheme, the mode $m_t = CA$ is chosen for comparison considering the corresponding state model's ability to deal with the highly manoeuvring vehicle.

The mean and standard deviation of RMSEs between the tracking results and ground truth trajectory for single and the multiple movement mode scheme are presented in Table 3, from which we can see that a significant improvement (more than 50% over the mean of RMSEs) is obtained by considering multiple movement modes. Besides, the probabilities of the 'stop' and 'non-stop' movement modes are estimated and presented in Fig. 7. It is observed that modes with larger estimated probabilities at different time instances are consistent with the ground truth as in Fig. 4(b).

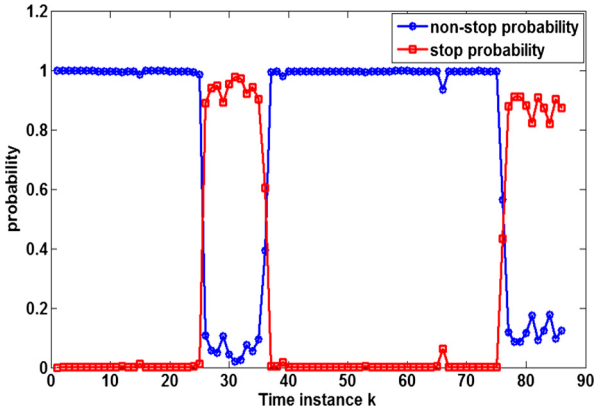

Fig. 7. The 50 times averaged stop/non-stop probabilities for every time instance.

Table 3
Performance comparison with different state model schemes for movement description.

	Mean (m)	Std (m)
Single movement model	25.82	5.73
Multiple movement models	11.07	1.15

4.4. Algorithm evaluation

Finally, we compare the proposed method with other particle filtering based algorithms including: VSMM-PF [10], VSMM-UPF [11] and the extension of the differential evolution-Markov chain particle filtering [19] for variable structure multiple models framework (VSMM-DEMC-PF). For a fair comparison, all the methods incorporate the GIS information by projecting invalid particles into the feasible region and the algorithms then become constrained versions of them (termed as C-VSMM-PF, C-VSMM-UPF, and C-VSMM-DEMC-PF).

The comparison of RMSEs between different algorithms are presented in Fig. 8 and Table 4. The performance of the C-VSMM-UPF and the C-VSMM-DEMC-PF is better than the C-VSMM-PF as they make use of measurement information for more effective particle generation. However, compared with those two, the proposed method (C-VSMM-PSO-PF) achieves even better performance as shown in Table 4. It also shows much higher computational efficiency than the C-VSMM-UPF. It is worthwhile noting that the proposed method achieves much better performance than C-VSMM-UPF when the vehicle stops (during 26–36 and 77–87 seconds) from Fig. 8(a). This is because when the vehicle stops, no measurements related to the vehicle will be received according to the characteristic of the GMTI radar. For the C-VSMM-UPF algorithm, only the mode transition probability and the state model are applied to obtain the mode and vehicle state. However, the PSO technique integrated in the proposed method makes the particles move to the high measurement likelihood region, which corresponds to the Doppler blind zone with small velocities. Besides, compared with the C-VSMM-DEMC-PF algorithm, the PSO algorithm makes use of the individual best *and* global best information to generate new populations, rather than generating new populations randomly as for the DEMC. In this way, more effective particles with high measurement likelihood values can be generated by the proposed C-VSMM-PSO-PF scheme.

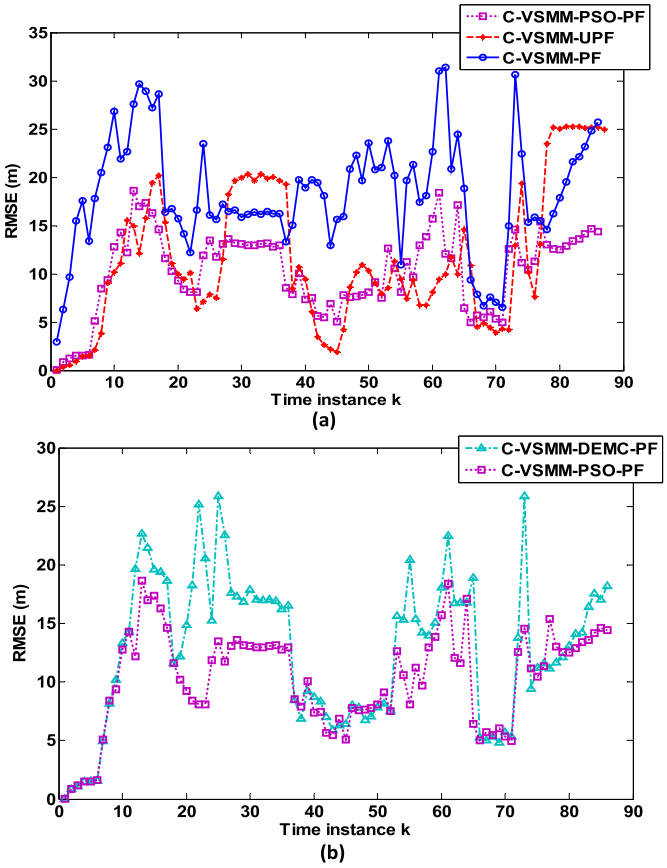

Fig. 8. The comparison of RMSEs at different time instances between different algorithms.

Table 4
The performance comparison for different estimation algorithms.

Algorithms	Mean (m)	Std (m)	Computation time (s)
C-VSMM-PF	19.14	2.90	3.18
C-VSMM-DEMC-PF	14.09	2.34	4.19
C-VSMM-UPF	13.94	1.72	18.14
C-VSMM-PSO-PF	11.07	1.15	4.30

5. Conclusions

This paper has proposed a novel method for manoeuvring ground vehicle tracking using a GMTI radar. It is considered that, in a realistic scenario, a ground vehicle's movement is constrained by the geographic conditions and it may manoeuvre in different modes. Comprehensive on/off road geographic information is exploited to constrain the movement of the tracked vehicle according to the environment, and multiple movement modes are applied to describe the vehicle manoeuvring on/off roads. Based on these geographic information and multiple movement modes, the C-VSMM-PSO-PF algorithm is proposed, which incorporates the PSO scheme into the particle filtering to obtain more effective particles by exploiting the measurement information. Comprehensive numerical simulations on a realistic scenario are performed to demonstrate the advantages of the proposed method.

Conflict of interest statement

There is no conflict of interest.

Acknowledgements

This work was supported by the UK Engineering and Physical Sciences Research Council (EPSRC) and the Ministry of Defence (MOD) University Defence Research Collaboration in Signal Processing under the grant number EP/K014307/1.

References

[1] R. Sullivan, Radar Foundations for Imaging and Advanced Concepts, SciTech Publishing Inc., 2004.
[2] H. Oh, S. Kim, H. Shin, A. Tsourdos, B. White, Behaviour recognition of ground vehicle using airborne monitoring of UAVs, Int. J. Syst. Sci. 45 (12) (2014) 2499–2514.
[3] B. Ristic, S. Arulampalam, N. Gordon, Beyond the Kalman Filter: The Particle Filters for Tracking Applications, Artech House, Norwood, MA, 2004.
[4] E. Mazor, A. Averbuch, Y. Shalom, J. Dayan, Interacting multiple model methods in target tracking: a survey, IEEE Trans. Aerosp. Electron. Syst. 34 (1) (1998) 103–123.
[5] Y. Boers, J. Driessen, Interacting multiple model particle filter, IEE Proc. Radar, Sonar Navig. 150 (5) (2003) 344–349.
[6] H. Oh, S. Kim, A. Tsourdos, Road-map assisted standoff tracking of moving ground vehicle using nonlinear model predictive control, IEEE Trans. Aerosp. Electron. Syst. 51 (2) (2015) 975–986.
[7] M. Ulmke, W. Koch, Road-map assisted ground moving target tracking, IEEE Trans. Aerosp. Electron. Syst. 42 (4) (2006) 1264–1274.
[8] Y. Cheng, T. Singh, Efficient particle filtering for road-constrained target tracking, IEEE Trans. Aerosp. Electron. Syst. 43 (4) (2007) 1454–1469.
[9] M. Yu, C. Liu, W. Chen, J. Chambers, A Bayesian framework with auxiliary particle filter for GMTI based ground vehicle tracking aided by domain knowledge, in: Proc. of SPIE, Signal Processing, Sensor/Information Fusion, and Target Recognition XXIII, Baltimore, MD, USA, 2014.
[10] M. Arulampalam, N. Gorden, M. Orton, B. Ristic, A variable structure multiple model particle filter for GMTI tracking, in: Proceedings of the Fifth International Conference on Information Fusion, Annapolis, MD, USA, 2002.
[11] O. Payne, N. Gordon, A. Marrs, An unscented particle filter for GMTI tracking, in: 2004 IEEE Aerospace Conference, Big Sky, Montana, USA, 2004.
[12] X. Zhang, W. Hu, S. Maybank, A smarter particle filter, in: 9th Asian Conference on Computer Vision, Xi'an, Chian, 2009.
[13] M. Wachowiak, R. Smolikova, Y. Zheng, J. Zurada, A. Elmaghraby, An approach to multimodal biomedical image registration utilizing particle swarm optimization, IEEE Trans. Evol. Comput. 8 (3) (2004) 289–301.
[14] S. Bhattacharjee, P. Mitra, S. Ghosh, Spatial interpolation to predict missing attributes in GIS using semantic kriging, IEEE Trans. Geosci. Remote Sens. 52 (8) (2014) 4771–4780.
[15] T. Kirubarajan, Y. Bar-Shalom, Tracking evasive move-stop-move targets with a GMTI radar using a VS-IMM estimator, IEEE Trans. Aerosp. Electron. Syst. 39 (3) (2003) 1098–1103.
[16] B. Vo, B. Vo, A. Cantoni, Bayesian filtering with random finite set observations, IEEE Trans. Signal Process. 56 (4) (2008) 1313–1326.
[17] X. Shao, B. Huang, J. Lee, Constrained bayesian state estimation: a comparative study and a new particle filter based approach, J. Process Control 20 (2) (2010) 143–157.
[18] https://www.ordnancesurvey.co.uk/business-and-government/products/opendata-products.html, accessed in September 2015.
[19] M. Du, X. Nan, L. Guan, Monocular human motion tracking by using DE-MC particle filter, IEEE Trans. Image Process. 22 (10) (2013) 3852–3865.